Annals of Nuclear Energy 142 (2020) 107426

Contents lists available at ScienceDirect

Annals of Nuclear Energy

journal homepage: www.elsevier.com/locate/anucene

Three dimensional reactor power profile reconstruction using Cerenkov radiation

Jason A. Hearne, Pavel V. Tsvetkov

Texas A&M University, Department of Nuclear Engineering, United States

ARTICLE INFO

Article history:
Received 26 November 2019
Received in revised form 17 February 2020
Accepted 23 February 2020
Available online 5 March 2020

Keywords:
Reactor instrumentation
Power profile
Cerenkov radiation
Flux mapping
TRIGA

ABSTRACT

The purpose of this study is to extend a method of power profile reconstruction based upon Cerenkov radiation measurements outside of a reactor core to provide information about the 3D power profile. Multiple simulated viewpoints above a coolant channel in a TRIGA reactor are used to estimate the axial tilt in the power density in the surrounding pins. The ability to produce a map of the axial flux tilts throughout the core is demonstrated. The presence of control rods inserted from the top of the core causes a downwards tilt throughout the reactor. Various reactor states are analyzed to demonstrate the ability of the method to provide information about changes in the axial flux tilt by comparing a perturbed state to a baseline.

1. Introduction

In previous work developing a method of 2D power profile determination using visual instrumentation through Cerenkov radiation detection (Hearne and Tsvetkov, 2020a–c), all Cerenkov estimates were for the light detected directly above the coolant channel, with no shadowing caused by the channel. As the number of detectors to be used is not fixed, the approximation could be valid or very close to accurate if horizontal distance between the coolant channel's center and the detection point is small, or corrections could be made. The information that can be gained from a detector above a coolant channel is limited to the total amount of Cerenkov coming from the channel, with no axial determination, restricting the information to a 2D map of the core. To include axial dependence and gain 3D information using visual detectors above the core, a method that compares the Cerenkov flux in a single channel observed from different positions can be used.

A few other methods of using Cerenkov radiation measurements for instrumentation in reactors have been developed, both historically (Rippon, 1963) (Lovvorn, 1961) (Weiss, 1965), and more recently (Arkani & Gharib, 2007) (Arkani & Gharib, 2009) (Bentoumi, et al., 2018) (Holschuh & Marcum, 2019) (Salles, et al., 2018) (Mesquita, et al., 2019). These other works are more experimental in nature and focus on determining the power level of the reactor as a whole but none of them incorporate spatial power profile determination from Cerenkov light produced in the coolant.

2. Modeling of detectable Cerenkov radiation above core

This study involves the estimation of the Cerenkov radiation detectable above a 1 MW TRIGA reactor with a fuel pins arranged in a square lattice. The Cerenkov light detectable at a point 2 m above the core midplane and 1.8 m above the top of the fueled region is estimated using MCNP 6.11 Beta (Goorley, 2014). The MCNP models place energy dependent electron tallies in regions within each coolant channel. A response function was generated in (Hearne and Tsvetkov, 2020a–c) using MCNP 6.11 Beta's new visible photon transport and Cerenkov production features (Durkee & James, 2013). The response function gives the visible photon flux at a detection point above the core per unit of electron flux in the coolant channel within each spatial and energy bin. This response function was then used to relate the tallied electron flux to the detectable Cerenkov flux above each coolant channel, so that the full core model does not need to transport the visible photons. The response function itself only depends on the properties of the water and size of the coolant channel, so it was calculated once only. The electron fluxes in the channels are tallied for each reactor state and would be updated for different rod positions, power levels and fuel burnup conditions. Each monitored coolant channel has an electron flux tally in a 1 cm radius cylindrical region of the channel, split into 16 axial segments and 23 electron energy bins. Each spatial and energy bin for the electron flux tally a coolant

E-mail address: jasonhearne@email.tamu.edu (J.A. Hearne)

https://doi.org/10.1016/j.anucene.2020.107426
0306-4549/

channel provides a contribution to the Cerenkov detected above the core; the total Cerenkov from a channel is the sum over all the contributions, as seen in equation (1):

$$\Psi_{Visible}(\boldsymbol{r},\boldsymbol{s}) = \sum_{n=1}^{Ebins}\sum_{m=1}^{Segments} \Phi_{Electron}(z_m, E_n)\Sigma_{Response}(z_m, E_n) \quad (1)$$

where $\Psi_{Visible}$ $(\boldsymbol{r},\boldsymbol{s})$ is the visible Cerenkov flux at a location above the coolant channel, $\Phi_{\mathrm{Electron}}(z_m, E_n)$ is the electron flux for axial segment m of the coolant channel and electron energy bin n, and $\Sigma_{Response}(z_m, E_n)$ is the value of the response function for the specific spatial and energy bins m and n.

A 9x9 grid of coolant channels are tallied to produce a 2D map of the Cerenkov light detectable above the core. A 2D plot of the TRIGA core showing the coolant channels that contain electron flux tallies can be seen in Fig. 1. The location of the origin and a compass showing the x and y directions is shown at the top of the plot.

3. Use of multiple viewpoints and shadowing for 3D extrapolation

An observation position that is horizontally offset from the coolant channel's center will observe more of the light from the top of the channel and less of the light from the bottom, due to the fuel pins blocking the light from reaching the detector. The left side of Fig. 2 shows how an offset viewpoint can have axial dependence for light detected from a channel, where the grey shaded region is the portion of the coolant channel that is "seen by" and contributing to the Cerenkov flux in the offset detector. For simplicity, the offset position analyzed is chosen such that exactly half of the total volume of the channel is visible; corresponding to a 7 cm offset 2 m above the core midplane. Also, for the shadowing effects, an approximation is made that treats the coolant channels and fuel pins as rectangular prisms is used to make the shadowing effects simpler, shown in the right side of Fig. 2. Some error may be introduced by this approximation, and a more rigorous, reactor specific treatment of the geometry shadowing of the channel at an offset viewpoint should be used if this system is to be implemented. The square channel approximation is only used in determining the Cerenkov contributions for different axial segments of

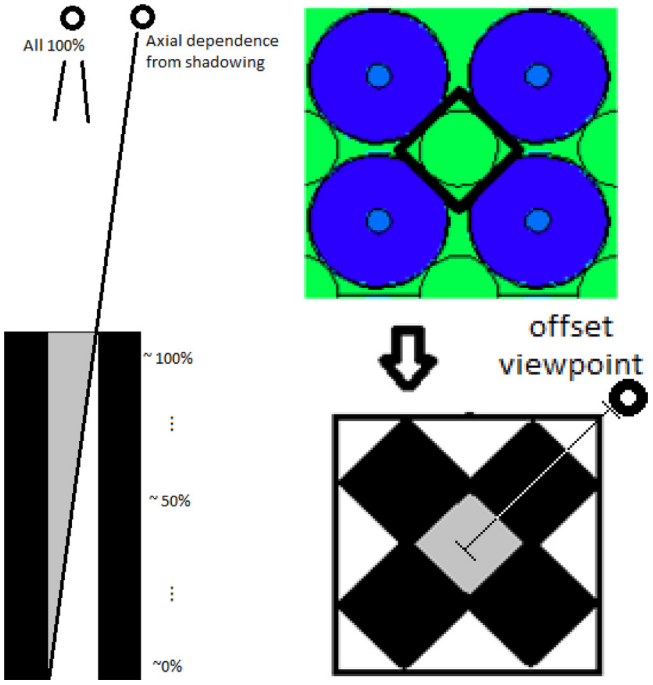

Fig. 2. Coolant channel segment contribution to Cerenkov observed at an offset from the channel centerline (left), where the shaded region is the only portion contributing to the signal at the offset location. Also, (right) the square coolant channel shadowing approximation, showing how the coolant channel and pins are approximated as square with an offset viewpoint perpendicular to the flat face of the square channel to simplify the geometry.

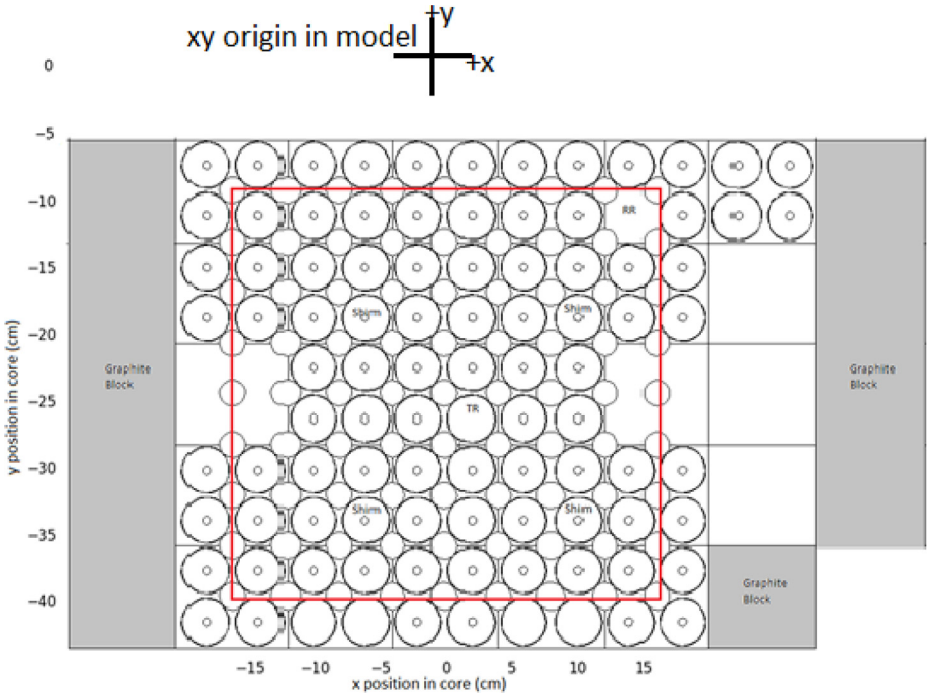

Fig. 1. XY cross section of core showing coolant channels tallied, as well as the control rod positions. The safety shims, transient rod (TR) and regulating rod (RR) positions are labeled. The red box corresponds to the region containing the coolant channels covered in the Cerenkov maps. (Hearne and Tsvetkov, 2020a–c). (For interpretation of the references to color in this figure legend, the reader is referred to the web version of this article.)

the coolant channel and does not otherwise affect the model or neutronics in any way.

The amount of light detected at the offset position is calculated using the same python script and method as is used for the detectors directly above the channel, except that there are modifications to the contributions from each axial segment. As in (Hearne and Tsvetkov, 2020a–c), the total is calculated by summing the contributions of the electron tally bins using the segment and energy specific electron to Cerenkov correlation factors. The modification is that for the offset viewpoint, each segment is also multiplied by its contribution factor, a number between 0 and 1, to account for shadowing. This is a modification to equation (1) and can be seen in equation (2):

$$\Psi_{offset} = \sum_{n=1}^{Ebins} \sum_{m=1}^{Segments} \Phi_{Electron}(z_m, E_n)\Sigma_{Response}(z_m, E_n) * \chi_{contribtion}(z_m) \quad (2)$$

The contribution factor, $\chi_{contribution}$ of a given segment to the offset detector's total is calculated using equation (3):

$$Segmentcontributionfactor = \chi_{contribution} = \frac{volumeofsegment\,visible}{total\,volumeofsegment} \quad (3)$$

The square channel approximation makes this a simple and consistent calculation to perform. The contributions for four of the 16 segments can be seen in Fig. 3. The top segment, bottom segment and the two middle segments are shown along with the upper and lower bounds of the segment are denoted by red lines and text. The grey shaded area shows the region that is contributing to the offset viewpoint's Cerenkov flux. The top and bottom segments are slightly smaller than the other segments due to the channel length not being a multiple of the segment size.

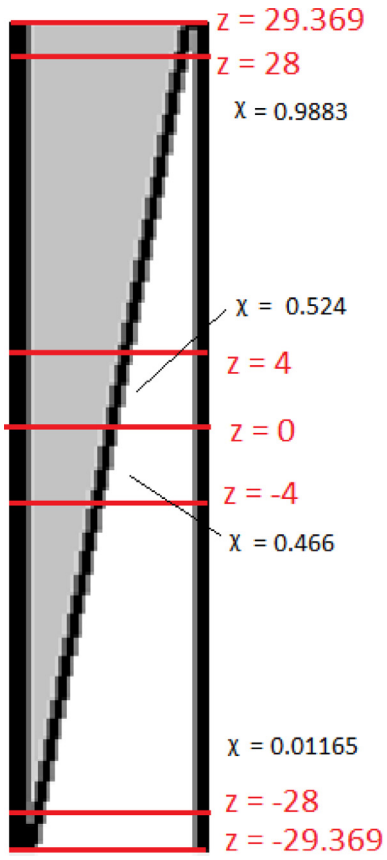

Fig. 3. Contribution factors for the top, two middle and bottom segments in the coolant channel.

This model uses the idealized square channel and an exact offset viewpoint that perfectly divides the square prism shaped coolant channel along a diagonal plane. In a real system, the segment contribution factors could be different for each channel and the offset viewpoints would be limited to the locations that have detectors. To reduce the required number of detectors, the detector directly above one coolant channel could be used as the offset detector above another, depending on the type, number and spacing of the detectors and fuel rods. Also, the system could use a single camera type detector as the detector positioned close to "directly above" many separate channels, correcting for the small shadowing effects. This could allow a close to direct viewpoint and a more substantially offset viewpoint to be used for every channel using a relatively small number of detectors by taking advantage of the fact that a detector above one channel is at an offset from another channel. Determining the offset factors involved for many different viewpoint offsets and more realistic channel shapes would require somewhat rigorous geometric calculations and is not a part of this research effort, as its focus is as a proof of concept, rather than a finalized design for production and usage.

One other advantage to the method of using contribution factors to determine the observed Cerenkov flux at an offset position is that the calculations can be done without requiring the MCNP model to be run again. The transport of photons and electrons is computationally expensive, so avoiding having to run additional input files improves the rate that progress can be made

The energy spectrum of the Cerenkov radiation produced in the coolant and then detected above the core has some slight dependence on the energy of the electrons and the distance through which the light has to travel in the coolant. Some of the higher energy UV photons are only produced by higher energy electrons, due to the index of refraction of water dropping to one as photon frequency increases into the harder UV range (Segelstein, 1981). Also, the transmission rate for hard UV light through water is lower than for visible light, so the effects of attenuation are more pronounced. For a detection point 2 m above the core midplane, the expected number of electron energy dependent UV photons is very low due to attenuation. There is some potential for using the spectrum of detected light to also provide axial information, as the light produced in the segments of the channel closer to the detector would have a slightly higher energy spectrum; however, distinguishing a spectrum with acceptable uncertainties using MCNP substantially increases the computational requirements and is outside the scope of this work. The total of all visible Cerenkov light is used for all of the response function tallies and for all total detector response calculations.

4. Axial Cerenkov tilt determination

The primary method of extracting axial information from the comparison of different Cerenkov detection points above the core is the calculation of an axial flux tilt for a coolant channel. The ratio of the offset Cerenkov flux to the flux directly above the channel provides information about whether the flux is shifted towards the top or bottom of the channel.

The segments near the top of the channel already contribute slightly more to the total Cerenkov above the core because they are closer to the tallying plane and thus have less loss due to the exponential attenuation caused by absorption and scattering and smaller losses to the $1/r^2$ light spreading effect. For this reason, even if the flux was perfectly symmetric about the axial centerline, the offset ratio will not be exactly 0.5, but instead will be some

value slightly above 0.5. To determine what the symmetric baseline axial tilt is, the model with 4 pins in an infinitely reflected lattice is used. This model has no control rods or other perturbations that will shift the flux either up or down, so the neutron population should be very close to symmetric in the axial direction. In the 4 pin reflected model the Cerenkov flux directly above the channel was 5.462E-6 and the offset flux was 2.866E-6, both in units of photons per cm^2 per second per source neutron in the 4 pin model. Using Eq. (4), the resulting flux tilt ratio is 0.5248. The flux tilt value of 0.5248 will therefore be used as a zero actual tilt baseline for the flux tilt in the whole-core models. This is used in Eq. (5) to obtain the absolute flux tilt for any channel, such that an axially symmetric flux has zero tilt, as seen here:

$$Axialoffsetratio = fluxtiltratio = \frac{Cerenkovdetectionatoffsetposition}{Cerenkovdirectlyabovechannel} \quad (4)$$

$$absolutetilt = fluxtiltratio - symmetrictiltratio \quad (5)$$

It is expected that most if not all of the absolute flux tilts will be negative (the ratio is below 0.5248), because of the presence of absorbers in the top portion of the core from the various control rods. If the fuel composition was heterogeneously burned, it could result in positive axial flux tilts, but heterogeneous burnup of fuel is not incorporated in the model used for tracking electrons. Most of the analysis of flux tilts will focus on changes in the tilt when the state of the reactor is altered, so when comparing two states, positive changes in the tilts will still occur.

For the flux tilt analysis of reactor state changes, the normal critical case is used as a baseline. In this state regulating rod is at 19.8 cm (49.5% withdrawal), the shims are at 28.4 cm (71% withdrawal), the transient rod is fully withdrawn, and the coupler box is not close to the core. A plot showing the flux tilt ratio normalized to the infinite lattice symmetric flux baseline for each coolant channel can be seen in Fig. 4. This plot is a plot of the flux tilt ratio except that the values has been shifted downward by 0.5248. In the plot of the flux tilt for the reactor in the normal state, every coolant channel has a negative absolute tilt as expected. The additional downward shift from local changes caused by each of the 4 safety shims can be seen in the 4 bluish depressions around the center of the plot. The partially inserted regulating rod also causes a notable downward flux tilt seen in the top right corner of the plot. The rest of the periphery of the reactor has a less pronounced tilt due to the lack of any nearby elements that are axially asymmetric. The scale for the color bar in Fig. 4 is the absolute tilt from Eq. (5), and is thus a unitless quantity. A tilt of zero means it is identical to the symmetric case, a more negative tilt means that it is shifted downwards more.

The normal state flux tilts are used as a baseline to determine tilt changes using Eq. (6):

$$changeintilt = perturbedtiltratio - baselinetiltratio \quad (6)$$

Changes do not need to be normalized to the symmetric case, as the normalization would cancel itself out due to subtraction.

5. State change analysis of axial tilts

In this section, various reactor state changes are modeled to show how the axial Cerenkov flux tilt will respond to the change. The goal is to demonstrate the ability of the Cerenkov flux tilt measurements to detect changes in the axial fission rate density and neutron population. The state changes are all compared to the normal critical state mentioned above. The altered states have the same total core power and the same fuel burnup; only the position of control rods and the graphite coupler box are changed. The comparison in the tilt in each channel is done using Eq. (6). The color scale used for plotting the tilt difference is changed from the rainbow scale used previously to a blue-white-red scale so that zero change is represented by white, and a darker blue or red represents a larger downward or upward flux shift.

The first perturbed state analyzed is the withdrawal of the regulating rod. The regulating rod is completely withdrawn from its initial position at 19.8 cm (49.5%) to 40 cm (100%). The safety shims are slightly inserted to compensate for the reactivity change. The regulating rod has a low reactivity worth, so the shims are only moved from 28.4 (71%) to 26.9 cm (67.25%). The flux tilt plot with the regulating rod withdrawn can be seen in Fig. 5. There is no longer a large negative flux tilt in the top right corner because the regulating rod is not causing increased absorption near the top of the core. The four downward tilt peaks near the shims are still present.

The difference plot that compares the flux tilts in with the regulating rod removed and with it in the baseline state can be seen in Fig. 6. The large upward shift in the flux tilt in the top right clearly shows the effect of the motion of the regulating rod. The upward shift only affects the region around the rod. The changes in the rest of the plot are much smaller, the largest being approximately 1/3

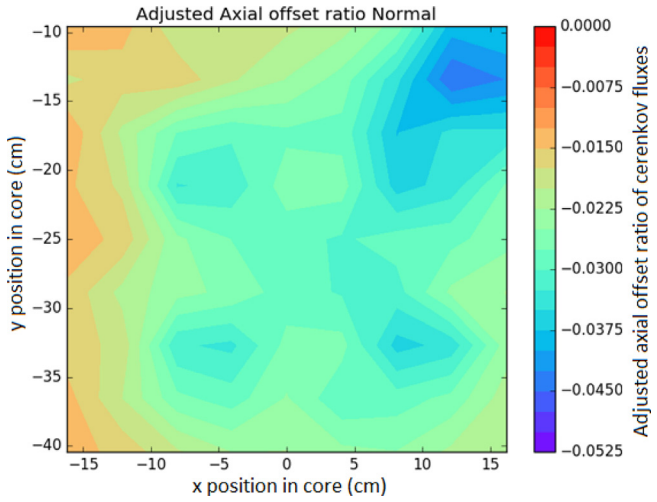

Fig. 4. Absolute tilt normalized to symmetric channel for each of the 81 coolant channels analyzed. The reactor is in the normal critical state.

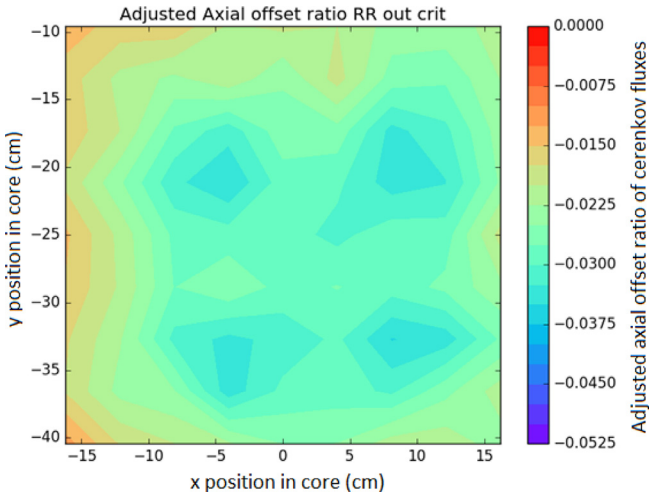

Fig. 5. Flux tilt map with regulating rod fully withdrawn.

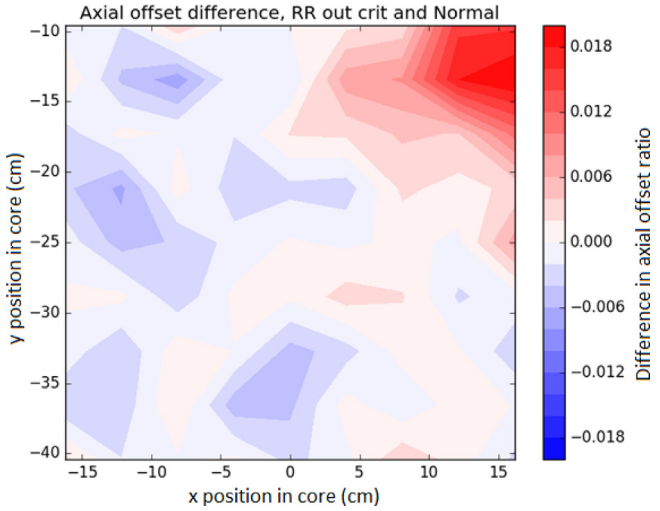

Fig. 6. Change in flux tilt when removing the regulating rod and slightly inserting safety shims to maintain criticality.

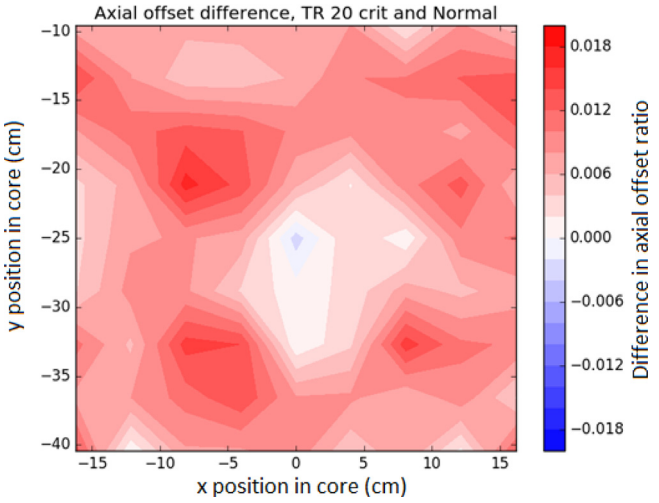

Fig. 8. Change in the flux tilt when inserting the transient rod to 20 cm and withdrawing the shims accordingly.

the magnitude of the shift near the regulating rod. Aside from the slight overall negative shift caused by the shims, the changes in the rest of the plot are due to uncertainty in the simulation.

A second perturbation involving the partial insertion of the transient rod is also modeled to observe how it changes the flux tilt. This rod movement involves inserting the transient rod to a position of 20 cm, corresponding to 50% withdrawal. The safety shims are almost completely withdrawn, being moved from their normal state position of 28.4 cm (71%) to 36.8 cm (92%) to compensate for the reactivity loss when inserting the transient rod. The regulating rod remains at 19.8 cm (49.5%). With the shims almost completely withdrawn, they have relatively little effect on the flux tilt. The flux tilt plot for the reactor in this state can be seen in Fig. 7. The distinctive low points in the tilt caused by the shims in the previous plots cannot be seen here, though there is now a depression in the center of the plot caused by the transient rod. The depression caused by the regulating rod is still present. The difference plot can be seen in Fig. 8. Most of the difference plot is red, corresponding to an upwards shift in the flux through most of the reactor. This is most pronounced in some of the channels near the shims that have been withdrawn. There is a negative shift in the Cerenkov flux tilt in one channel next to the transient rod, but it would appear that the insertion of the transient rod has a much smaller effect on the overall axial flux tilt than the compensatory removal of the shims.

The movement of the core such that it is next to the graphite coupler is also analyzed for its effects on the axial flux tilt. The coupler box is a large graphite block that is used to push neutrons into beam ports, the coupler box next to the core can be seen in Fig. 9. The graphite of the coupler box is a much better neutron reflector than the open expanse of light water that is normally bordering that face of the core, so this motion causes a large reactivity insertion, requiring the safety shims to be inserted to a position of 17 cm (43%), compared to their initial position of 28.4 cm (71%). This creates a horizontal flux tilt that can be seen in Fig. 10. Note that Fig. 10 shows the proportional difference in the total Cerenkov flux above each channel, similar to the plots in (Hearne and Tsvetkov, 2020a–c), not the axial flux tilt.

With such a large change in the total flux near the north portion of the core (the top of the plots), it is interesting to note that this is not at all shown in the flux tilt plots. The change in the axial offset is plotted in Fig. 11. There is a slight downward shift in the flux tilt in the central region of the core where the effects of the shim insertions are present. The top of the plot shows little to no shift in the axial offset, in contrast to the more than 20% increase in the total

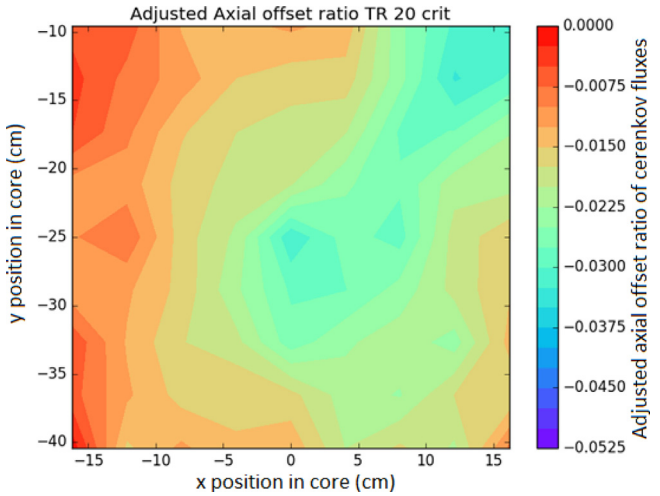

Fig. 7. Flux tilt in each channel when the transient rod is halfway inserted and the shims moved further out to maintain criticality.

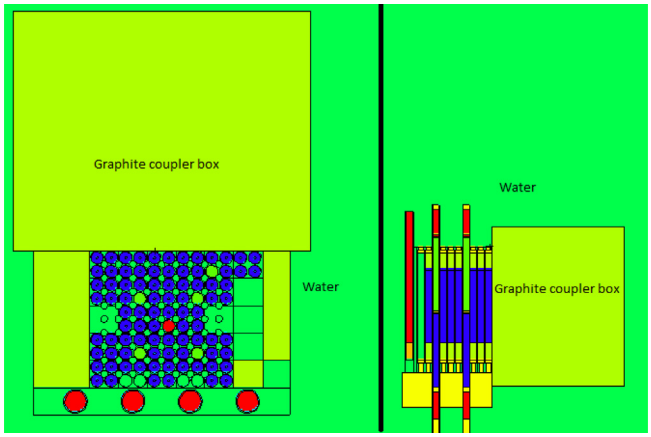

Fig. 9. Reactor core when moved next to coupler box, showing XY (left) and YZ (right) views of the core.

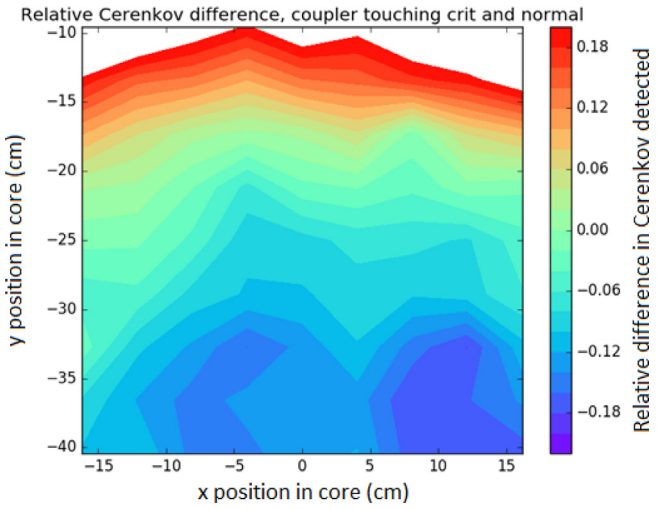

Fig. 10. Relative change in the total Cerenkov flux directly above each channel when moving the coupler box next to the core and inserting shims to maintain criticality. The white space above the plot indicates a greater than 20% increase in the total Cerenkov flux. (Hearne and Tsvetkov, 2020a–c).

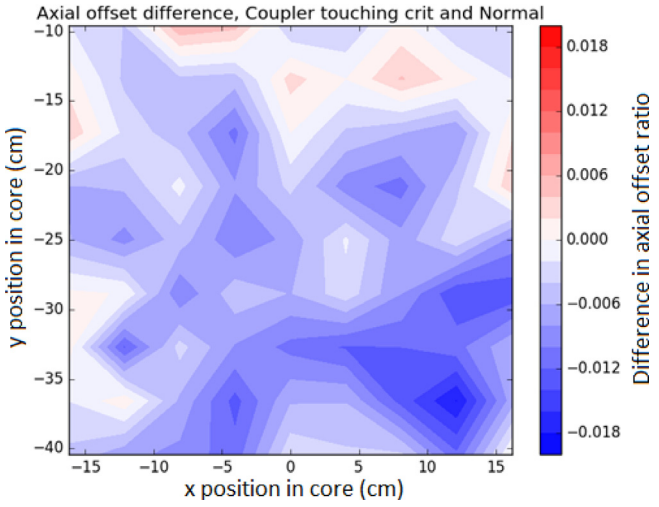

Fig. 11. Change in flux tilt when moving the core next to the graphite coupler box.

flux seen above. This is an indication that the change in that region is more or less axially symmetrical. This is the case, because the change in the boundary condition uniformly affects the entire axial length of the fuel pins. The graphite block extends above and below the ends of the pins, so edge effects at the top and bottom are minimal.

Comparing the changes in the total flux and the changes in the axial tilt can determine whether the cause of the change is affecting the entire height of the core equally or if it is focused on the top or bottom half. Distinguishing between a uniform change and one that is not uniform but is still axially symmetric; however, would require more offset viewpoints for each channel and more complex analysis methods than those employed in this research effort.

6. Conclusions

The potential for the use of Cerenkov radiation detection multiple viewpoints above a coolant channel as a form of instrumentation for obtaining information about the 3D power profile for a reactor has been demonstrated. Axial tilts in coolant channels across the core provide information about where the electron and gamma fluxes in the coolant are the highest and thus which nearby regions have the highest fission densities. The ability to detect and identify various reactor state changes is shown.

This spatial power profiling method could provide more information about the fission densities and fluxes in the core, potentially allowing for improved optimization of fuel shuffling, better characterization of hot channel factors, or the detection of some flux shifting anomalies such as xenon oscillations. This could be applied to quickly detect and locate physical anomalies such as a blocked coolant channel, as demonstrated in (Hearne and Tsvetkov, 2020a–c).

7. Disclaimer

This paper was prepared as an account of work sponsored by an agency of the United States Government. Neither the United States Government nor any agency thereof, nor any of their employees, makes any warranty, expressed or implied, or assumes any legal liability or responsibility for the accuracy, completeness, or usefulness of any information disclosed.

Any views, opinions, findings, conclusions, or recommendations expressed in this publication are those of the authors and do not necessarily state or reflect the views of the Department of Energy Office of Nuclear Energy.

CRediT authorship contribution statement

Jason A. Hearne: Conceptualization, Methodology, Software, Formal analysis, Investigation, Writing - original draft, Writing - review & editing, Visualization. **Pavel V. Tsvetkov:** Supervision, Project administration, Funding acquisition, Writing - review & editing.

Declaration of Competing Interest

The authors declare that they have no known competing financial interests or personal relationships that could have appeared to influence the work reported in this paper.

Acknowledgements

This research is being performed using funding received from the DOE Office of Nuclear Energy's Nuclear Energy University Program, NEUP Award Number DE-NE0008306.

Appendix A. Supplementary data

Supplementary data to this article can be found online at https://doi.org/10.1016/j.anucene.2020.107426.

References

Arkani, M. & Gharib, M., 2007. Design and Construction of an Independent Channel for Tehran Research Reactor Power Measurement Using Cherenkov Detector. s. l.:M. S. Thesis, Azad University, Research and Science Department, Tehran.

Arkani, M., Gharib, M., 2009. Reactor core power measurement using Cherenkov radiation and its application in Tehran research reactor. Ann. Nucl. Eng. 36, 869–900.

Bentoumi, G. et al., 2018. Reactor power monitoring using Cherenkov radiation transmitted through a small-bore metallic tube. Ann. Nucl. Energy 114, 86–91.

Durkee, J.W., James, M.R., 2013. MCNP6 Cerenkov Radiation Feature Verification. Los Alamos National Lab, Los Alamos, New Mexico.

Goorley, T., 2014. MCNP6.1.1-Beta Release Notes, s.l. Los Alamos National Lab.

Hearne, J.A., Tsvetkov, P.V., 2020a. Physical anomaly detection and identification using Cerenkov radiation. Ann. Nucl. Energy 142, 107424.

Hearne, J.A., Tsvetkov, P.V., 2020b. Response function generation for cerenkov radiation production and transport in a TRIGA coolant channel. Ann. Nucl. Energy 138, 107200. https://doi.org/10.1016/j.anucene.2019.107200.

Hearne, J.A., Tsvetkov, P.V., 2020c. Spatial power profiling method using visual information in reactors with optically transparent coolants. Ann. Nucl. Energy 137, 107071. https://doi.org/10.1016/j.anucene.2019.107071.

Holschuh, T., Marcum, W., 2019. The CRANK System—A Simple, Robust Apparatus for Measurement of Cherenkov Light at Open-Pool Reactor. Nucl. Technol. 8, 1–7.

Lovvorn, J.L., 1961. Reactor power monitor utilizing Cerenkov radiation. IRE Trans. Nucl. Sci. 8 (4), 3–5.

Mesquita, A.Z., Salles, B.M., Luciano, M.R., 2019. Design of a visual system to monitoring thermal power in pool-type nuclear research reactor. Int. J. Adv. Eng. Res. Sci. 6 (3), 243–248.

Rippon, S.E., 1963. Cherenkov detectors for the measurement of reactor power. Nucl. Ins. Methods 21, 192–196.

Salles, B.M., Mesquita, A.Z., Luciano, M.R., 2018. Development of a research reactor power measurement system using cherenkov radiation. ACCENTS Trans Image Process Computer Vision (TIPCV) 4 (13), 33–38.

Segelstein, D.J., 1981. The complex refractive index of water. University of Missouri, Kansas City.

Weiss, H., 1965. Power measurement and automatic reactor control by gamma - or cerenkov - radiation. Vienna, Austria, s.n., pp. 461-474.